water

MDPI

Article

Turbulence Characteristics before and after Scour Upstream of a Scaled-Down Bridge Pier Model

Seung Oh Lee [1] and Seung Ho Hong [2,*]

[1] Department of Civil Engineering, Hongik University, 94 Wausan-ro, Mapo-gu, Seoul 04066, Korea
[2] Department of Civil and Environmental Engineering, West Virginia University, 1306 Evansdale Drive, Morgantown, WV 26506, USA
* Correspondence: sehong@mail.wvu.edu

Received: 19 August 2019; Accepted: 9 September 2019; Published: 12 September 2019

Abstract: Bridge pier scour is one of the main causes of bridge failure and a major factor that contributes to the total construction and maintenance costs of bridge. Recently, because of unexpected high water during extreme hydrologic events, the resilience and security of hydraulic infrastructure with respect to the scour protection measure along a river reach has become a more immediate topic for river engineering society. Although numerous studies have been conducted to suggest pier scour estimation formulas, understanding of turbulence characteristics which is dominant driver of sediment transport around a pier foundation is still questionable. Thus, to understand near bed turbulence characteristics and resulting sediment transport around a pier, hydraulic laboratory experiments were conducted in a prismatic rectangular flume using scale-down bridge pier models. Three-dimensional velocities and turbulent intensities before and after scour were measured with Acoustic Doppler Velocimeter (ADV), and the results were compared/analyzed using the best available tools and current knowledge gained from recent studies. The results show that the mean flow variable is not enough to explain complex turbulent flow field around the pier leading to the maximum scour because of unsteady flows. Furthermore, results of quadrant analysis of velocity measurements just upstream of the pier in the horseshoe vortex region show significant differences before and after scour.

Keywords: bridge pier; horseshoe vortex; Physical hydraulic modeling; quadrant analysis; Scour and Velocity field

1. Introduction

Bridge pier scour is one type of local scour caused by sediment transport that is driven by local flow structure; therefore, it is necessary to be acquainted with the flow structure and the related scour mechanisms around the bridge pier. In general, the local flow structure around a bridge pier is composed of downflow at the upstream face of the pier in the vertical plane; the horseshoe vortex system that wraps around the base of the pier, which is the primary contributor to local scour upstream of the pier; the bow wave near the free surface on the upstream face of the pier; and the wake vortex system at the rear of the bridge pier that extends over the flow depth [1–3]. These features greatly complicate the understanding of the local flow structures [4,5], and the comprehensive effect of those complex flow structures is to increase the local sediment transport leading to additional local scour around the bridge pier [6,7].

When flow approaches a bridge pier, the velocity becomes zero on the upstream face of the bridge pier. Due to the strong adverse pressure gradient imposed by the bridge pier in the streamwise approach flow direction, the boundary layer separates upstream of the bridge pier. In the separated region, several vortices are consecutively developed, and subsequently stretched around the base of the bridge pier, giving rise to what is called a horseshoe vortex system. The primary horseshoe vortices

rotate in the same sense as the approach boundary layer vorticity, but secondary vortices have the opposite rotation to preserve streamline topology. During the time that the horseshoe vortex nearest the bridge pier is decreasing in size due to stretching, a newer and younger secondary separation vortex is induced upstream of the primary vortex. The size and strength of the secondary horseshoe vortex increases with time while the size of the primary vortex continues to be reduced by stretching. At some time, the secondary and smaller vortices merge with the primary horseshoe vortex or leapfrog it to strengthen the primary horseshoe vortex, which is finally stretched completely around the bridge pier temporarily stabilizing the flow. Subsequently, instability occurs and the primary vortex forms again. The process is then repeated irregularly [8,9].

In addition to the theoretical descriptions of local vortex structures, to find more general relationships between the vortex system around a bridge pier and the resulting sediment transport, many researchers have adopted analytical, experimental, as well as computational approaches. Melville [10] has observed that the size and circulation of the horseshoe vortex increases rapidly, and the velocity near the bottom of the hole decreases as the scour hole is enlarged. According to Melville, magnitude of the downflow seems to be directly associated with the rate of scour. However, Baker [11] argued that because the size of the scour hole is much larger than the size of the vortex core on a flat-bed before scouring, such a calculation would predict wrongly that the circulation increases as scour proceeds. In his study, Baker [11] used the horseshoe vortex core circulation to derive an equation to predict the scour depth. Baker [11] assumed that the horseshoe vortex strength in the scour hole can be equal to that on a flat-bed as scour depth develops and suggested the equation with respect to pier width and free stream velocity. Later, Nakagawa and Suzuki [12] assumed that the scale and strength of the primary horseshoe vortex are constant during evolution of the local scour hole and suggested a scour prediction equation with using the stochastic nature of particle movement, originally developed by Einstein [13]. At similar time, Qadar [14] experimentally hypothesized the maximum scour depth to be a function of the initial vortex strength which is composed of vortex size and stream velocity. Based on the experimental results, an envelope curve was proposed to show the relationship between scour depth and initial vortex strength. Qadar [14] quantitatively evaluated his results by comparing with laboratory and field data.

After Qadar [14], Kothyari et al. [15] explored the diameter of primary vortex using a regression analysis of experimental data on flow around a cylindrical pier. They mentioned that the diameter of the primary vortex is dependent on the bridge opening width in comparison to the size of pier diameter. Also, Ram [16] expressed an equation for initial diameter of the horseshoe vortex and, in his findings, the initial diameter of the vortex decreases with increasing the pier Reynolds number (Re_b) represented by a pier width as a characteristics length. However, Muzzammil and Gangadhariah [17] found that the relative vortex size, which is the ratio of vortex diameter and pier width, is weakly influenced by the pier Reynolds number for higher values on a rigid flat bed. This means that vortex size is only dependent on the pier width for higher values of the pier Reynolds number ($Re_b > 10^4$). Based on analytical models relating scour depth to horseshoe vortex properties, Muzzammil and Gangadhariah [17] proposed that equilibrium scour depth is a function of the horseshoe vortex size, tangential velocity, and vortex strength in the scour hole. They found that the mean size of the horseshoe vortex is ~20% of the cylindrical pier diameter, and the vortex tangential velocity is ~50% of the mean velocity of approach flow for $10^4 \leq Re_b \leq 1.4 \times 10^5$ at fixed flat-bed conditions. The size of the vortex is assumed to be independent of the sediment mobility.

More recently, Dey and Raikar [7] found that the flow and turbulence intensities in the horseshoe vortex in a developing scour hole are reasonably comparable with those in before scour. Similar results can be found in other studies conducted with large-eddy simulations (LES) and detached-eddy simulation (DES) [18–20]. However, based on the experimental studies using particle image velocimetry (PIV), Guan et al. [21] argued that the size of the main vortex responsible for the maximum scour depth upstream of the pier increases with increasing scour depth.

In clear-water scour regime, as the scour depth increases, the shear stress beneath the horseshoe vortex is reduced until the shear stress becomes less than the critical shear stress and sediment movement ceases in the scour hole. As explained in the previous paragraphs, even if the role, size, and strength of turbulence leading to pier scour have been investigated qualitatively, the coherent turbulent characteristics and associated bursting events for sediment transport is still an active area of interest. So far, several of methods presented in literatures for describing the horseshoe vortex properties have not considered turbulent characteristics or unsteadiness of the horseshoe vortex; but, in fact, the bed materials around a bridge pier move irregularly in time even if the approach flow is steady. It is found in the literature that the strength and size of the horseshoe vortex are closely related to the pier geometry and the approach flow velocity upstream of the bridge while the scour depth cannot be accurately predicted unless a clear relationship between the large-scale unsteadiness of the horseshoe vortex and sediment size is presented quantitatively. One of the important objectives of this study is investigating turbulence characteristics and sequential occurrence of bursting turbulence events before and after scour in the process of particle entrainment in front of a pier. Thus, to comprehensively attack the objectives, hydraulic laboratory experiments were conducted in a flume using two different scaled-down bridge pier models. Visual observations by high speed camera as well as three-dimensional velocities and turbulent intensities before and after scour measured with ADV were analyzed using the best available tools and current knowledge.

2. Methodology

2.1. Experimental Setup

As shown in Figure 1a,b, in previous studies [22–24], laboratory experiments were conducted using various scaled hydraulic model of the Chattahoochee River bridge at Cornelia, Georgia, and Flint River bridge at Bainbridge, Georgia, USA, respectively, including the full river bathymetry. The previous experimental studies successfully explored the effect of sediment size on pier scour depth at different geometric model scales and, also based on the large number of experimental and field investigations/comparisons, improved local scour formulas were suggested. Furthermore, strategies of deciding sediment size for scaled-down hydraulic modeling was also proposed. After those model studies, each pier bent were carefully removed from the laboratory flume. Figure 1c,d show example of bridge pier bent model of Chattahoochee River bridge and Flint River bridge, respectively, with individual scales for this study. Pier bent consists of four rectangular concrete columns and rectangular concrete footings for Chattahoochee River bridge, as shown in Figure 1c. However, for Flint River bridge, two square concrete pier columns are placed on large stepped square concrete footings.

The removed pier bent model shown in Figure 1c,d was re-built inside a 1.1 m wide by 24.4 m long glass-sided tilting flume to investigate detailed turbulence and flow characteristics in front of the pier before and after scour. The approach section of the pier model was 15.0 m long followed by a working mobile bed section with a length of 3.0 m in which the pier model was placed. The length of the approach section was decided based on the findings from other researches [25–29] to ensure a fully developed approach turbulent flow and turbulent boundary layer at the bridge pier. After the working mobile bed section, additional 3 m long sediment trap section downstream of the pier model was placed. For the current set of experiments, instead of using actual cross section shape and river geometry used in the previous experiments, the channel was constructed to have a straight alignment rather than meandering, and rectangular shape of cross section was maintained through the entire flume to find more general features of flow and turbulence fields. The flume was filled with 0.53 mm bed sediment for each experiments and carefully leveled to the elevations established by the field measurements in each site. Figure 2a, b show experimental setup before running scour experiment for Chattahoochee River bridge model and Flint River bridge model, respectively.

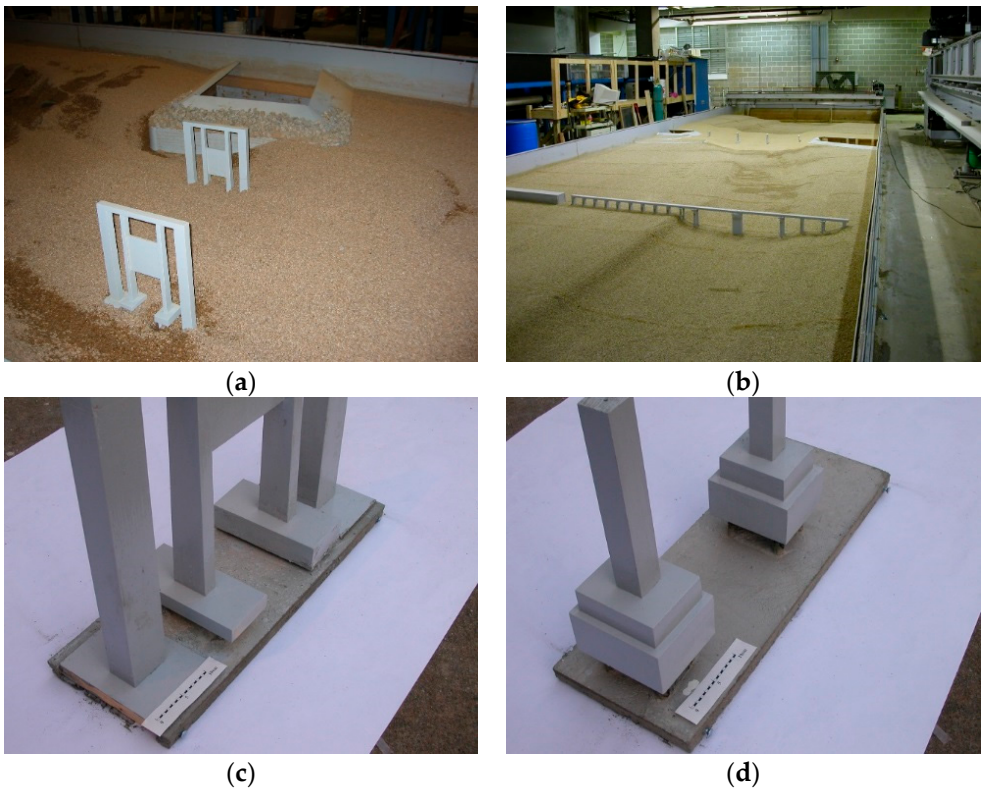

(**a**) (**b**)

(**c**) (**d**)

Figure 1. Hydraulic laboratory model in previous laboratory studies and bridge pier model for this study: (**a**,**c**) 1:23 scaled model for Chattahoochee River bridge and (**b**,**d**) 1:33 scaled model for Flint River bridge.

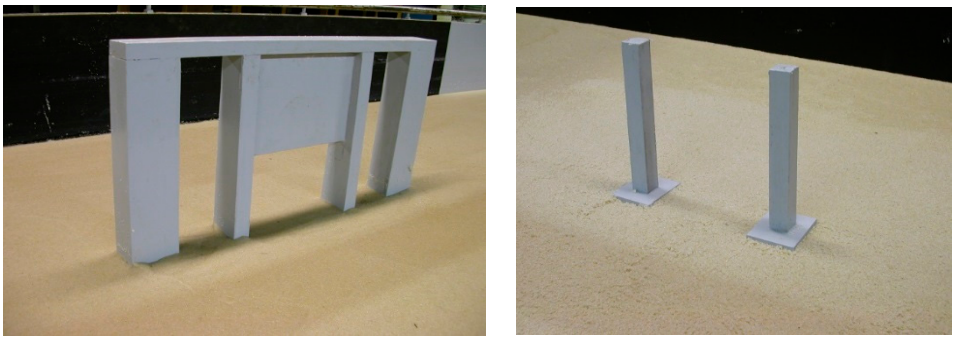

(**a**) (**b**)

Figure 2. Pier model in the flume: (**a**) Chattahoochee River bridge model and (**b**) Flint River bridge model.

2.2. Experimental Procedure

The experimental campaign consists of two scenarios: moveable bed experiment and fixed-bed experiment. First, moveable bed experiments were conducted to investigate variance of hydraulic parameters affecting scour depth over time. The flume was slowly filled with water to saturate the sand. After complete saturation, the required discharge (uncertainty of $\pm 2.8 \times 10^{-4}$ m^3/s) was established with the flow depth adjusted well above the desired value. Then, the flow depth was gradually decreased by changing the height of the tailgate until the target approach flow depth was obtained. During this time, the point gage (uncertainty of $\pm$ 1 *mm*) was used to monitor the flow depth. Once the target flowrate and the flow depth had been reached, scour continued for 2 to 3 days until equilibrium was achieved. The equilibrium was defined when the increment of scour depth is less than 5% of

the bride pier diameter during 24 h. During the scouring process, instantaneous point velocities and turbulence quantities were measured by ADV in front of the pier. Furthermore, temporal change of bed elevations were measured periodically using ADV temporarily positioned for a moment above the point of scouring. At the end of scouring (equilibrium state), the velocity flow field was measured throughout the test section both in the near field next to the pier and in the far field at relative elevations for the comparison of turbulence and flow characteristics between after scour and before scour. During the velocity measurements, ADV sampling frequency was chosen to be 25 Hz with a duration of at least 2 min and perhaps as much as five minutes depending on the magnitude of turbulence at each measuring location. The correlation values in these measurements were greater than 80% and the Signal Noise Ratio (SNR) was greater than 15. The phase-space despiking algorithm was also employed to remove any spikes in the time record caused by aliasing of the Doppler signal which sometimes occurs near a boundary. More detailed filtering protocol can be found in Lee and Sturm [22] and Hong et al. [26]. After the completion of each experiment, the final bed elevations were measured using the ADV and the point gage.

When the moveable bed experiments were completed, the entire moveable bed was re-leveled and fixed by spraying polyurethane. During fixed-bed experiments, the same flow conditions as those in moveable bed experiments were reproduced, and velocities and turbulence quantities were measured in the same way as in the moveable bed experiments to investigate the effect of initial flow parameters responsible for the scour. In addition to the measurements of initial flow parameters, flow visualization experiments were also conducted. A kaolinite suspension was used as a tracer upstream of the bridge pier to show the flow structure around the bridge pier and also to detect the frequency of the horseshoe vortex system immediately upstream of the pier. The tracer was transferred from a conical tank by an electric pump operating at a maximum flowrate of 0.003 m^3/s. The kaolinite suspension was mixed to achieve a concentration of 1.0 mg/cm^3 in the tank. The flow rate of tracer was adjusted with the aid of rotameter to produce a released velocity that was the same as the open channel mean velocity. As the tracer was released at a constant rate, a high speed video camera (30 FPS) was used to capture the unsteady dynamics of the swirl of the horseshoe vortex as it amplified and partially collapsed in size.

3. Results and Discussion

The experimental conditions have been summarized in Table 1, where Q is the total discharge, b is the width of bridge pier, y_1 is approach section water depth, V_1 is approach section velocity, T_{eq} is time to the equilibrium scour, and d_s is the equilibrium scour depth in front of the bridge pier.

Table 1. Summary of measured experimental conditions.

Run	Model	Scale	Q (m^3/s)	b (m)	y_1 (m)	V_1 (m/s)	T_{eq} (h)	d_s (m)	Conditions
1	CR	1:23	0.051	0.046	0.191	0.257	30	0.093	Fixed &
2			0.044	0.046	0.142	0.304	12	0.090	Moveable-bed
3	FR	1:33	0.054	0.055	0.241	0.215	48	0.046	Fixed &
4			0.052	0.055	0.170	0.281	24	0.085	Moveable-bed

CR: Chattahoochee River bridge model and FR: Flint River bridge model.

3.1. Velocity Field

The velocity fields around the pier bent were measured for the Chattahoochee River model and Flint River model in both the fixed-bed (before scouring) and moveable-bed (after scouring in equilibrium). Figure 3a,c shows the velocity fields of "before scour" for Run 1 and Run 3, respectively. The longitudinal distance (x) and lateral distance (y) were normalized with width of corresponding bridge pier model and the near field vectors measured at 40 percent of the approach flow depth were normalized by measured approach velocity. Higher velocities were shown on both sides of the first

pier, where deeper scour occurred as the flow curved around the pier bent. In the wake zone, the mean velocities became smaller than those in the outer region. The velocity defected in this region gradually recovered in the downstream direction. The magnitude of mean velocities upstream of the first pier along the centerline became smaller approaching the pier stagnation line due to the existence of the pier. Figure 3b,d shows the combination of scour depth contours and the near-field velocities measured at 40 percent of the approach flow depth under the same flow condition as in "before scouring" but at the completion of scour for Run 1 and Run 3, respectively. The near-field velocity distributions were very close to being symmetric with respect to the centerline of the bridge pier bent as shown in Figure 3 for both runs. The characteristic decrease in magnitude was observed in near field velocity around the pier bents when comparing results before and after scour. The maximum relative difference in magnitude was approximately 30–40 percent for both cases in the vicinity of the first pier on the right-hand side. Interestingly, the maximum scour depth occurred at the nose of front pier for Run 1, as expected, however for the case of Run 3, the maximum scour occurred between the two piers with a high degree of symmetry on the left and right sides as shown in Figure 3d. For the Flint River bridge pier bent, the pier columns are placed on large stepped footings and the footings are already exposed at the beginning of scour as shown in Figure 2b. Because the footing intercepts the downflow along the nose of pier bent which feeds the size and strength of horseshoe vortex, the amount of local scour depth in front of the first pier was reduced [30–32].

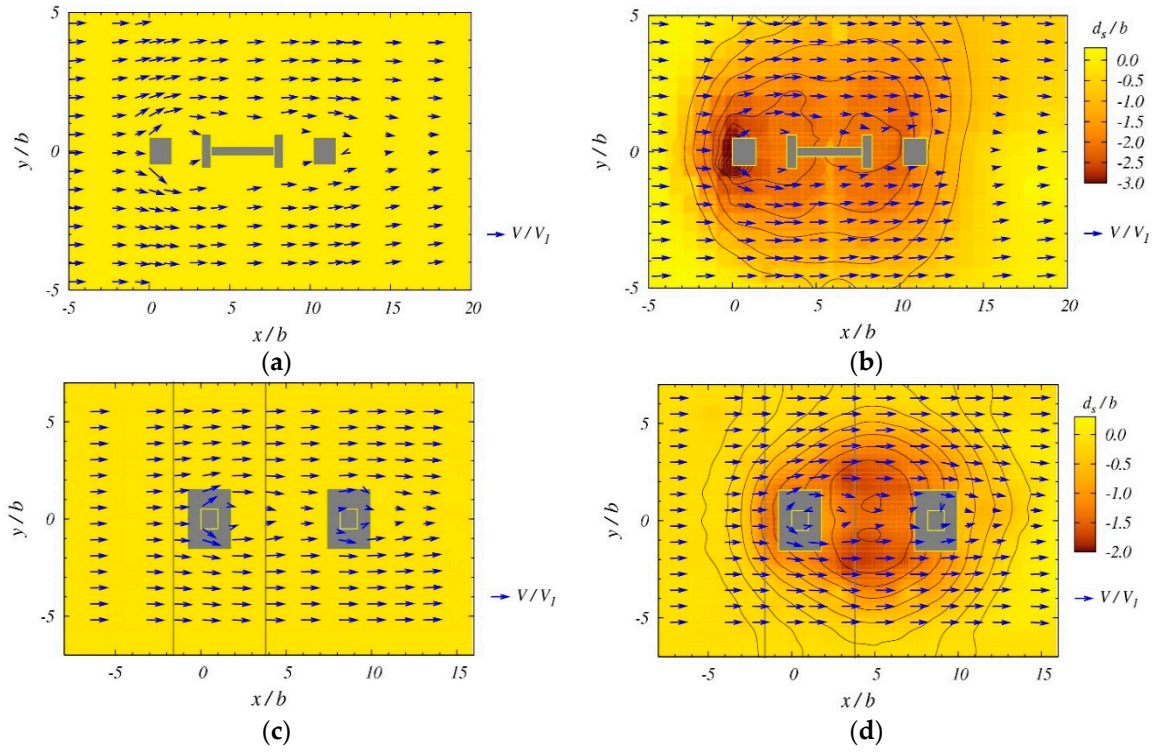

Figure 3. Normalized mean velocity vectors: Measured at 40 percent of the approach depth for experimental Run 1 before and after scour in (**a**,**b**), respectively, and Run 3 before and after scour in (**c**,**d**), respectively.

3.2. Temporal Variation of Flow and Turbulence Characteristics Upstream of the Bridge Pier

The measured mean velocity and turbulence kinetic energy (TKE) fields have been usually used to validate three-dimensional numerical models. Even though the simulated velocity profiles at several locations were in good agreement compared with the laboratory experiments, quantitative connections with the scour depth are difficult to make. In addition, results from a three-dimensional numerical model show that the maximum mean shear stress on a fixed bed does not correspond with

the maximum depth of scour hole in front of the piers [33]. Furthermore, as shown in Figure 3, the horizontal mean (time-averaged) point velocity vector plots did not indicate large changes in the velocity field with scour development when comparing the before- and after-scour conditions. It is concluded that the details of the horseshoe vortex itself must be investigated further to understand the development of the scour hole in front of the pier rather than the general-mean turbulence and flow characteristics of the near field.

Thus, in an effort to better understand the relationship between the flow field and the resulting pier scour over the development of scour hole, bed elevations, and three-dimensional velocity components as well as turbulence intensities upstream of the bridge pier were measured intermittently at two points during the scour process to capture the temporal variation of flow and turbulence characteristics as the scour hole developed. The flow was continued for the measurements so that the measurements could be completed in a time duration that was short (approximately 2–3 min) in comparison to the rate of scour hole development. The two measured points were located horizontally at a distance of one pier width upstream of the bridge pier in the streamwise direction because the size of horseshoe vortex is comparable with the size of pier width. As shown in Figure 4, the vertical location of one point (*LOC*1) was in the scour hole itself where it was varied to maintain a constant vertical displacement above the bed as the scour hole deepened with time. The other point (*LOC*2) was fixed above *LOC*1 but at a constant elevation that was close to the initial bed elevation before scour began as also shown in Figure 4. Sufficient clearance between the bridge pier and the ADV probe was required in order to place the ADV probe without bumping the pier or disturbing the horseshoe vortex system upstream of the bridge pier. Thus, the Chattahoochee River bridge model was chosen for this experiment based on the physical size and simple footing shape compared to the Flint River model.

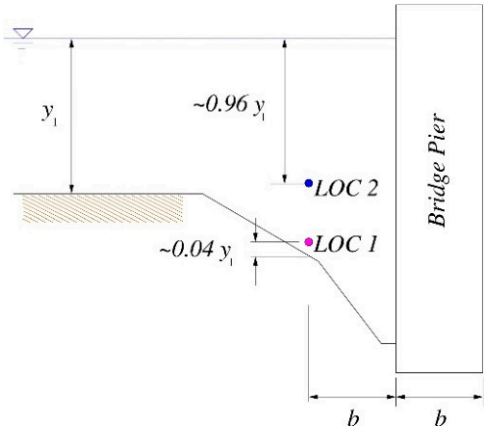

Figure 4. Schematic diagram of the locations for measuring the temporal variation of flow characteristics.

The streamwise (*U*) and vertical (*W*) time-averaged velocity profiles normalized by approach mean velocity at *LOC*1 and *LOC*2 are shown in Figure 5. Both velocity profiles at *LOC*1 fluctuated slightly with time, but the values remained close to zero as the scour depth increased over time which is shown on the secondary vertical axis in Figure 5a. The averaged values became close to zero at *LOC*1 since it is located near the bed in the separation zone. However, the velocity profiles at *LOC*2 fluctuated significantly with time as shown in Figure 5b because the vertical position of *LOC*2 moved into the highly turbulent region associated with the horseshoe vortex during development of the scour hole. The fluctuations in the streamwise velocity seem to be associated with the intermittent fluctuations in the scour hole depth that result from the collapse of the sides of the hole, followed by further scouring as the hole enlarges.

The turbulence intensity in both the streamwise (u') and vertical (w') directions at *LOC*1 increased during the initial stage of scour development and then became smaller with time as shown in Figure 6a. The large fluctuations of streamwise turbulence intensity during the initial stages of scour development

is due to the unsteadiness of the location of the separation point upstream of the pier. As the scour depth changed rapidly during the initial stage, the vertical turbulence intensity became approximately four times larger than at later stages of scour hole development, indicating that the contribution of vertical turbulence intensity to the rate of scour development was very significant during the initial stage. Figure 6b shows that the turbulence intensity in both vertical and streamwise directions at *LOC*2 approached the same constant value as the scour hole developed. The vertical turbulence intensity at *LOC*2 was relatively small at the beginning of the scour process, but then increased significantly to a value greater than that at *LOC*1. This is due to the movement of the vertical location of *LOC*2 into the highly turbulent region associated with the horseshoe vortex.

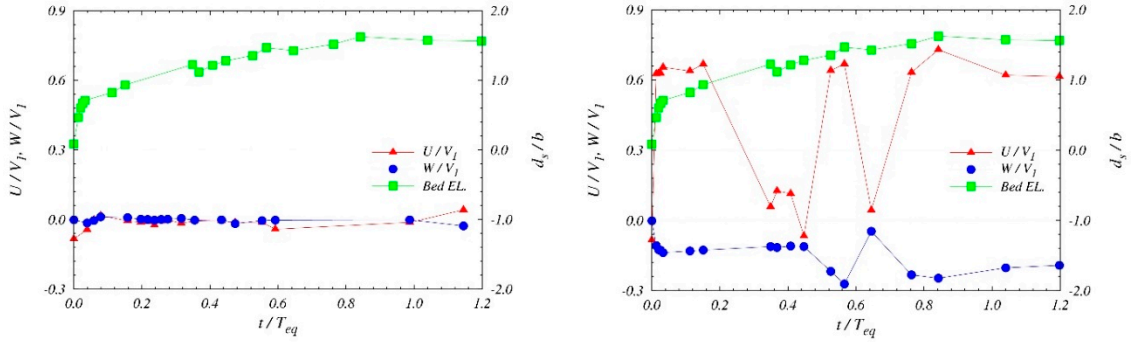

Figure 5. Velocity profile over time at (**a**) *LOC* 1 and (**b**) *LOC* 2 for Run 1.

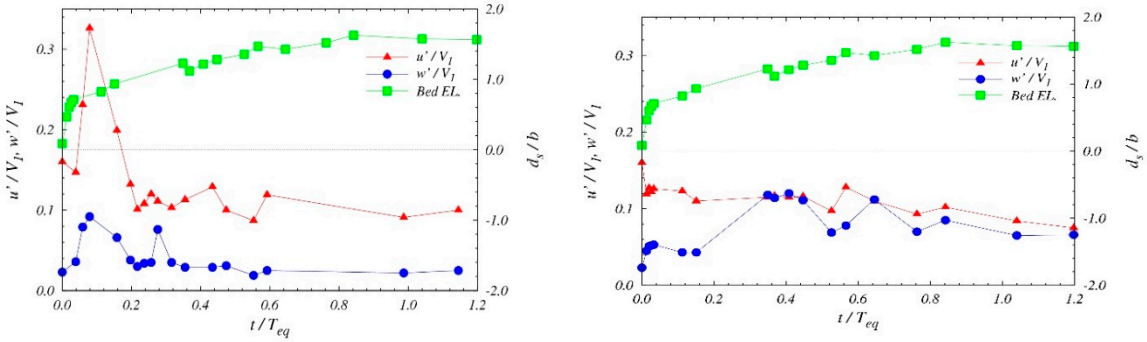

Figure 6. Temporal variations of turbulence intensity profile at (**a**) *LOC* 1 and (**b**) *LOC* 2 for Run 1.

3.3. Flow Characteristics Upstream of the Bridge Pier

While in the previous section, the long-term temporal development was considered in relationship to the variance of velocity and turbulence characteristics in the scour hole, this section investigates the short-term transient behavior of the flow immediately upstream of the bridge pier on a fixed flat bed in the region of flow separation and the horseshoe vortex. The primary horseshoe vortex is unsteady with the formation of a system of secondary vortices, and the secondary vortices are quasi-periodically combined with the primary vortex increasing its size and strength depending on the degree of stretching around the pier [8,9]. Thus, the primary horseshoe vortex oscillates in position and size in an irregular shift between two modes of behavior which are expanding and contracting over time. Those oscillation of horseshoe vortex in its size and strength in front of the pier was captured by high-speed camera in Figure 7 in this experiment, and the time difference (Δt) between Figure 7a,d was related to the frequency of horseshoe vortex [22,34]. As shown in Figure 7, because of those two modes, the instantaneous velocity time series when measured near the bed close to the pier alternately exhibits periods of positive streamwise velocity towards the pier followed by negative streamwise

velocity away from the pier. The result is a bimodal velocity distribution, first described by Devenport and Simpson [34], and further studied experimentally and numerically [18,22,35]. Those two alternate states of the horseshoe vortex are bistable with the contracted mode occurring approximately 20–30% of the time. Furthermore, they found that the shape, relative size, and distance between the two peaks of the bimodal probability density function of instantaneous velocities are not permanent and stable, but instead vary with the position of the velocity measurement.

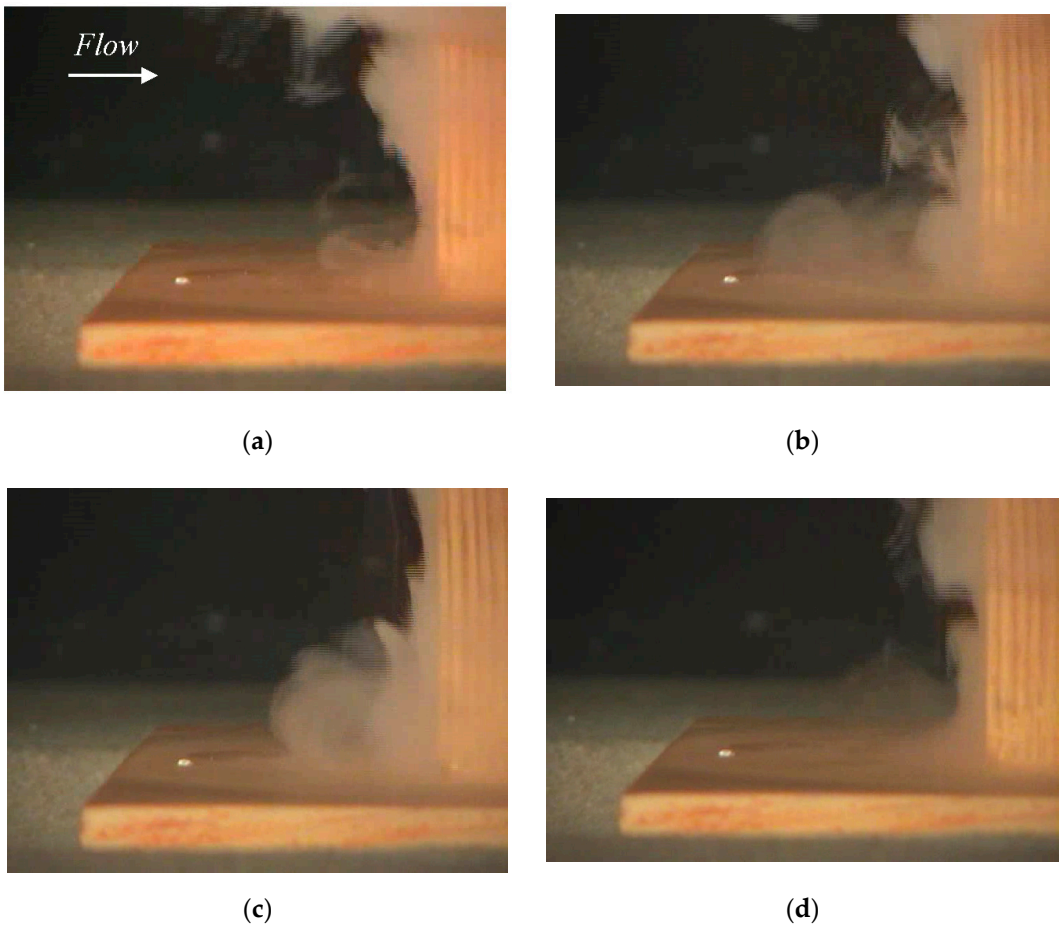

Figure 7. Flow visualization of horseshoe vortex with tracer injection in experimental Run 4: sequential snap shots from (**a**–**d**).

With respect to the turbulence characteristics just upstream of the pier in the horseshoe vortex region, quadrant analysis was also used to further characterize the turbulent events associated with the large-scale unsteadiness of the horseshoe vortex. Quadrant analysis was employed in this study by examining the joint probability density function of the streamwise and vertical components of fluctuating velocity, denoted as u' and w', respectively.

The four quadrants shown in Figure 8 correspond to four types of turbulent events which are defined as: I. outward interactions; II. ejections or bursts; III. inward interactions; and IV. sweeps that characterize the individual turbulent velocity measurements. The Reynolds stress is generally produced by all four types of events. The first quadrant event, I, is characterized by outward motion of high-speed fluid, with $u' > 0$ and $w' > 0$; the second quadrant event, II, is identified by outward motion of low-speed fluid, with $u' < 0$ and $w' > 0$, which is usually called ejection or bursts; the third quadrant event, III, is associated with inward motion of low-speed fluid, with $u' < 0$ and $w' < 0$; and finally, the fourth quadrant event, IV, represents the motion of high-speed fluid toward the bed, with $u' > 0$ and $w' < 0$, and it is called sweeps.

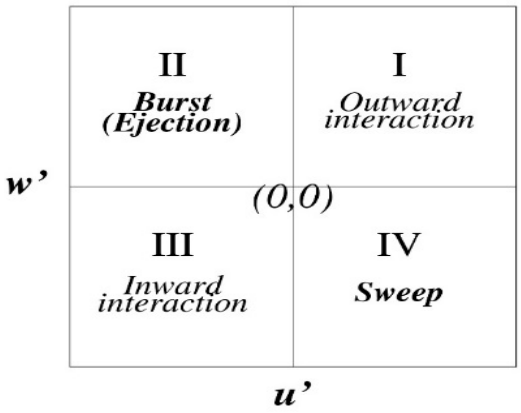

Figure 8. Schematic of the plate for quadrant analysis [36].

The relationships between the fluid motions and particle transfer near the wall can be elucidated through quadrant analysis. The ejections and sweeps contribute positively to the bed shear stress since $\overline{u'w'}$ is the flux of forward momentum to the bed, whereas the outward and inward interactions contribute negatively to the bed shear stress. The presence of a sweep corresponds to a local increase of the shear stress at the bed whereas the occurrence of an ejection corresponds to a local decrease of the shear stress at the bed. Therefore, the coherent sweep and ejection events appear to be responsible for transferring particles toward and away from the bed [37]. However, in nonuniform flows such as the wake region downstream of a backward-facing step, Keshavarzi et al. [36] have shown that turbulent events with the same shear stress contribute to different sediment transport rates due to the frequency structure of the turbulent events. While the horseshoe vortex is not expected to have the same turbulence structure as a turbulent wake, nevertheless, it does have the property of intermittency that is an important contributor to the scour process.

Among the velocity measurements made in experimental Run 2 and Run 4, two time series of velocity data at the nose of the pier were selected to conduct the quadrant analysis and to investigate the change of flow characteristics of the before-scour case and after-scour case. Figure 9 shows the results of Run 2. The time series analyzed in Figure 9a was measured for the fixed bed condition while the time series analyzed in Figure 9b was measured inside the scour hole under the same flow conditions at approximately the same distance above the bed. The joint probability density function in both figures are normalized to the peak values of 1.0, and it is necessary to multiply the contoured values by the scaling factors in the middle of the top of each figure to produce probability densities. The selected locations were both in the region of the horseshoe vortex and separated region upstream of the pier.

The results of quadrant analysis show a significant difference between the before-scour case and after-scour case in Figure 9a,b. The turbulent events for the before-scour condition were dominated by bursts and sweeps with a bimodal joint frequency distribution at the elevation of $z = 0.17\ b$. In Figure 9a before scour, sweeps events had a higher probability of occurrence, and for both types of events, the values of u' were greater than those of w' at the maximum probability of occurrence. Run 4 shows similar probability density patterns as in Figure 9. The bursts and sweeps are the primary forcing function for creating the scour hole because they both represent positive shear stress; however, the more important characteristic is the irregular oscillation between the two types of events as the horseshoe vortex alternately expands and contracts as the separation point moves back and forth, as shown in Figure 7. The sediment particles are lifted and entrained in an intermittent fashion as explained in Lee and Sturm [22]. In the equilibrium scour hole in Figure 9b, the turbulent events no longer display the bimodal distribution with all four types of events becoming approximately equally likely. The magnitude and frequency of all events are significantly affected by the change of the flow inside the scour hole. There is no effective event of the velocity fluctuations for altering the shear stress or moving the sediment out of the equilibrium scour hole. Although the existence of the bimodal

distribution depends on the measuring location, it is significant that it disappears near the bed after scour and at the same distance above the bed as for the before-scour case.

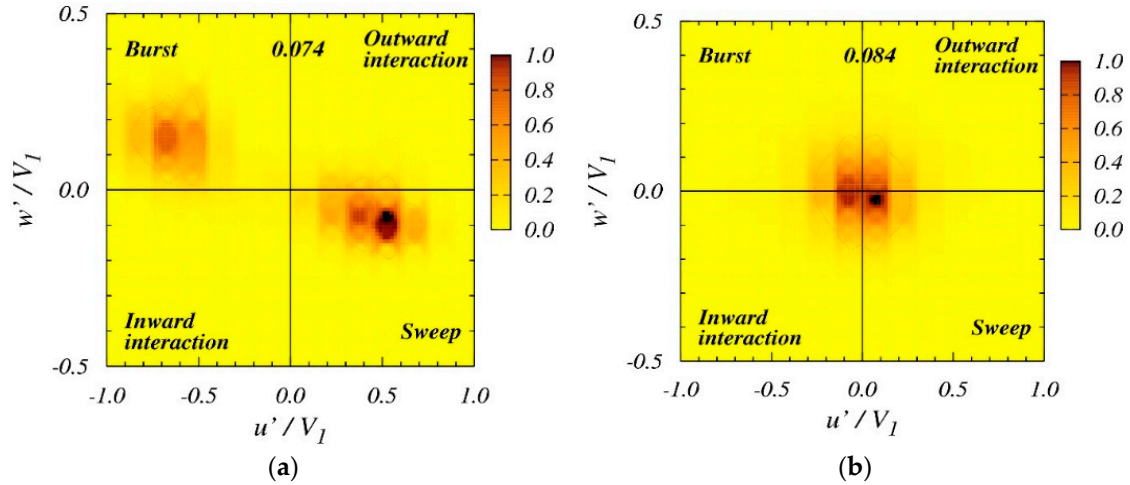

Figure 9. Joint probability density function of u' and w' for (**a**) before-scour case and (**b**) after-scour case measured at $x/b = -0.33$ and $z/b = 0.17$ for Run 2.

As a further indication of the differences in the turbulence properties as the scour hole develops, the integral time scale was computed for both the before-scour and after-scour time series associated with Figure 9. The integral time scale is defined as a measure of the time over which a velocity component is dependent on its past values and a rough measure of the time interval over which a fluctuating velocity component is highly correlated with itself; it is obtained by integration of the measured autocorrelation distribution over time and a measure of the memory of the process [38]. As given in Table 2, the integral time scale in the vertical direction for the before-scour case is considerably higher than for the after-scour case; whereas, in the streamwise direction, the time scale is the same order of magnitude for both cases. The vertical fluctuation in the before-scour case is a significant contributor to the processes of suspending and eroding sediment from the bed. Accordingly, a longer integral time scale of the velocity fluctuations gives more transport than a shorter integral time scale when the rate of sediment transport increases very rapidly at the initial stage of scour development.

Table 2. Comparison of integral time scales for before and after scour cases.

	Before Scour, Sec	**After Scour, Sec**
Streamwise direction	1.8	1.3
Vertical direction	4.3	0.7

4. Summary and Conclusions

Although local scour around bridge foundations have been extensively studied for several decades, there still remain problems because of difficulties in visualization and understanding the complex flow structure leading to scour. Thus, in this study, laboratory experiments were conducted with scaled-down bridge pier models for more complete descriptions of flow characteristics of the horseshoe vortex system around the complex bridge pier. During the experiments, velocities and turbulence intensities as well as the bed elevations before and after scour were measured by ADV. Furthermore, a simple visualization technique was used to capture the unsteadiness of horseshoe vortex. The results shows that horizontal velocity vector plot comparisons between before-scour and after-scour conditions measured at a certain relative height above the bed was not enough to explain the complex scour mechanism because the values were all temporally averaged ones, and so did not show the effects of the large-scale unsteadiness of the horseshoe vortex system upstream of a bridge pier. Further

investigation using the probability distribution of instantaneous velocity components and quadrant analysis of velocity fluctuations in the horizontal and vertical directions shows that the vertical and streamwise velocity components exhibited a bimodal probability distribution before scour near the bed upstream of the pier where horseshoe vortex is responsible for sediment transport. The streamwise and vertical velocity fluctuations were observed to be dominated by sweeps and bursts, both of which contribute positively to the bed shear stress and exhibit a bimodal joint frequency distribution. The bursts and sweeps are the primary forcing function for creating the scour hole at initial stage because they both represent positive shear stress. They are the result of irregular oscillation of the horseshoe vortex between two preferred states as the reverse flow near the bed in front of the pier either extends upstream or retreats to a point closer to the pier. As a result, the sediment particles are lifted and entrained in an intermittent fashion. After scour is complete, at equilibrium stage, the turbulent events no longer display a bimodal distribution near the bottom of the scour hole. Furthermore, a quantitative physical connection is made between the scour depth and the large-scale unsteadiness of the horseshoe vortex system in front of the pier by comparing time scales for lifting of the sediment particle, and subsequent entrainment and transport of the particle out of the scour hole.

Even if this study provides additional insights to better understand the local pier scouring process and the relationship between scour depth and the horseshoe vortex, the local flow structures in the field are affected by additional parameters, such as vertical and lateral flow contraction, unsteadiness of discharge during the passage of a flood event, and their interaction. Furthermore, in reality, scouring often happens under live-bed scour conditions with infilling of the scour hole as the flood recedes which is not well understood over a long time series because it is greatly affected by the conditions required to generally mobilize the entire bed and is further complicated by the movement of bed forms through the bridge section. Thus, additional well-designed physical model and field measurements as well as numerical simulations are required to investigate these effects, including the modeling of flow contraction, realistic hydrographs, and bed forms, such as dunes and ripples.

Author Contributions: S.O.L. designed/fabricated the scaled-down bridge model, and conducted the flume experiments; S.O.L. and S.H.H. provided descriptions and motivation, and analyzed the laboratory data; S.H.H. wrote the paper; all authors participated in final review and editing of the paper.

Funding: This research received no external funding.

Acknowledgments: This work was partially supported by the National Research Foundation of Korea (NRF) grant funded by the Korea government (MIST) (NRF-2017R1A2B2011990). Also, Seung Ho Hong was supported by West Virginia University for this study.

Conflicts of Interest: The authors declare no conflict of interest.

References

1. Graf, W.H.; Istiarto, I. Flow pattern in the scour hole around a cylinder. *J. Hydraul. Res.* **2002**, *40*, 13–20. [CrossRef]
2. Chang, W.; Lai, J.; Yen, C. Evolution of scour depth at circular bridge piers. *J. Hydraul. Eng.* **2007**, *130*, 905–913. [CrossRef]
3. Gautam, P.; Eldho, T.I.; Mazumder, B.S.; Behera, M.R. Experimental study of flow and turbulence characteristics around simple and complex pier using PIV. *Exp. Therm. Fluid Sci.* **2019**, *100*, 193–206. [CrossRef]
4. Dey, S. Sediment pick-up for evolving scour near circular cylinders. *Appl. Math. Model.* **1996**, *20*, 534–539. [CrossRef]
5. Khaple, S.; Hanmaiahgari, P.; Gaudio, R.; Dey, S. Interference of an upstream pier on local scour at downstream piers. *Acta Geophys.* **2017**, *65*, 29–46. [CrossRef]
6. Unger, J.; Hager, W. Down-flow and horseshoe vortex characteristics of sediment embedded bridge piers. *Exp. Fluids* **2007**, *42*, 1–19. [CrossRef]
7. Dey, S.; Raikar, R.V. Characteristics of horseshoe vortex in developing scour holes at piers. *J. Hydraul. Eng.* **2007**, *133*, 399–413. [CrossRef]

8. Dargahi, B. Turbulent flow field around a circular cylinder. *Exp. Fluids* **1989**, *8*, 12. [CrossRef]
9. Simpson, R.L. Junction flows. *Annu. Rev. Fluid Mech.* **2001**, *33*, 415–443. [CrossRef]
10. Melville, B.W. Local Scour at Bridge Sites. Ph.D. Thesis, School of Engineering, University of Auckland, Aukland, New Zealand, 1975.
11. Baker, C.J. Theoretical approach to prediction of local scour around bridge piers. *J. Hydraul. Res.* **1980**, *18*, 12. [CrossRef]
12. Nakagawa, H.; Suzuki, K. Application of stochastic model of sediment motion to local scour around a bridge pier. In Proceedings of the 16th Congress of the International Association for Hydraulic Research, Sao Paulo, Brazil, 24 July–6 August 1975; pp. 285–299.
13. Einstein, H.A. *Bed-load Function for Sediment Transportation in Open Channel Flows*; Bulletin 1027 71, United States Department of Agriculture (USDA): Washington, DC, USA, 1950.
14. Qadar, A. Vortex Scour Mechanism at Bridge Piers. *Proc. Inst. Civ. Eng.* **1981**, *71*, 739–757. [CrossRef]
15. Kothyari, U.C.; Garde, R.J.; Ranga Raju, K.G. Temporal variation of scour around circular bridge piers. *J. Hydraul. Eng.* **1992**, *118*, 1091–1106. [CrossRef]
16. Ram, S. A theroretical model to predict local scour at bridge piers in non-cohesive soils. In Proceedings of the The Seventh International Symposium on River Sedimentation, Hong Kong, China, 16–18 December 1998; pp. 173–178.
17. Muzzammil, M.; Gangadhariah, T. Caracteristiques moyennes d'un vortex en fer a cheval au droit d'une pile cylindrique(The mean characteristics of horsehoe vortex at a cylindrical pier). *J. Hydraul. Res.* **2003**, *41*, 285–297. [CrossRef]
18. Kirkil, G.; Constantinescu, S.; Ettema, R. Coherent structures in the flow field around a circular cylinder with scour hole. *J. Hydraul. Eng.* **2008**, *134*, 572–587. [CrossRef]
19. Kirkil, G.; Constantinescu, G. Flow and turbulence structure around an instream rectangular cylinder with scour hole. *Water Res. Res.* **2010**, *46*, W11549. [CrossRef]
20. Schanderl, W.; Jenssen, U.; Strobl, C.; Manhart, M. The structure and budget of turbulent kinetic energy in front of a wall-mounted cylinder. *J. Fluid Mech.* **2017**, *827*, 285–321. [CrossRef]
21. Guan, D.; Chiew, Y.; Wei, M.; Hsieh, S. Characterization of horseshoe vortex in a developing scour hole at a cylindrical bridge pier. *Int. J. Sediment Res.* **2019**, *34*, 118–124. [CrossRef]
22. Lee, S.; Sturm, T.W. Effect of sediment size scaling on physical modeling of bridge pier scour. *J. Hydraul. Eng.* **2009**, *135*, 793–802. [CrossRef]
23. Hong, S.; Lee, S. Insight of Bridge Scour during Extreme Hydrologic Events by Laboratory Model Studies. *KSCE J. Civ. Eng.* **2018**, *22*, 2871–2879. [CrossRef]
24. Lee, S.; Hong, S. Reproducing field measurements using scaled-down hydraulic model studies in a laboratory. *Adv. Civ. Eng.* **2018**, *2018*, 11. [CrossRef]
25. Hong, S.; Abid, I. Scour around an erodible abutment with riprap apron over time. *J. Hydraul. Eng.* **2019**, *145*, 6. [CrossRef]
26. Hong, S.; Sturm, T.W.; Stoesser, T. Clear water abutment scour in a compound channel for extreme hydrologic events. *J. Hydraul. Eng.* **2015**, *141*, 12. [CrossRef]
27. Saha, R.; Lee, S.; Hong, S. A comprehensive method of calculating maximum bridge scour depth. *Water* **2018**, *10*, 1572. [CrossRef]
28. Yoon, K.; Lee, S.; Hong, S. Time-averaged turbulent velocity flow field through the various bridge contractions during large flooding. *Water* **2019**, *11*, 13. [CrossRef]
29. Chua, K.; Fraga, B.; Stoesser, T.; Hong, S.; Sturm, T.W. Effect of bridge abutment length on turbulence structure and flow through the opening. *J. Hydraul. Eng.* **2019**, *145*, 19.
30. Ge, L.; Lee, S.; Sotiropoulos, F.; Sturm, T.W. 3D unsteady RANS modeling of complex hydraulic engineering flows. Part II: Model validation and flow physics. *J. Hydraul. Eng.* **2005**, *131*, 809–820. [CrossRef]
31. Jones, J.S.; Kilgore, R.T.; Mistichelli, M.P. Effects of footing location on bridge pier scour. *J. Hydraul. Eng.* **1992**, *118*, 280–290. [CrossRef]
32. Melville, B.W.; Raudkivi, A.J. Effects of foundation geometry on bridge pier scour. *J. Hydraul. Eng.* **1996**, *122*, 203–209. [CrossRef]
33. Coleman, S.E. Clearwater local scour at complex piers. *J. Hydraul. Eng.* **2005**, *131*, 330–334. [CrossRef]
34. Devenport, W.J.; Simpson, R.L. Time-dependent and time-averaged turbulence structure near the nose of a wing-body junction. *J. Fluid Mech.* **1990**, *210*, 23–55. [CrossRef]

35. Paik, J.; Escauriaza, C.; Sotiropoulos, F. On the bimodal dynamics of the turbulent horseshoe vortex system in a wing-body junction. *Phys. Fluids* **2007**, *19*, 045107. [CrossRef]
36. Keshavarzi, A.; Melville, B.; Ball, J. Three-dimensional analysis of coherent turbulent flow structure around a single circular bridge pier. *Environ. Fluid Mech.* **2014**, *14*, 821–847. [CrossRef]
37. Marchioli, C.; Soldati, A. Mechanisms for particle transfer and segregation in a turbulent boundary layer. *J. Fluid Mech.* **2002**, *468*, 283–315. [CrossRef]
38. Kundu, P.K. *Fluid Mechanics*; Academic Press: San Diego, CA, USA, 1990.